Bis(carbazol-9-ylphenyl)aniline End-Capped Oligoarylenes as Solution-Processed Nondoped Emitters for Full-Emission Color Tuning Organic Light-Emitting Diodes

Tanika Khanasa,[†] Narid Prachumrak,[†] Rattanawaree Rattanawan,[†] Siriporn Jungsuttiwong,[†] Tinnagon Keawin,[†] Taweesak Sudyoadsuk,[†] Thawatchai Tuntulani,[‡] and Vinich Promarak*[,§]

[†]Department of Chemistry and Center of Excellence for Innovation in Chemistry, Faculty of Science, Ubon Ratchathani University, Ubon Ratchathani, 34190 Thailand

[‡]Department of Chemistry, Faculty of Science, Chulalongkorn University, Bangkok, 10330 Thailand

[§]School of Chemistry and Center of Excellence for Innovation in Chemistry, Institute of Science, Suranaree University of Technology, Muang District, Nakhon Ratchasima, 30000 Thailand

Ⓢ *Supporting Information*

ABSTRACT: A series of bis(3,6-di-*tert*-butylcarbazol-9-ylphenyl)aniline end-capped oligoarylenes, BCPA-Ars, are synthesized by double palladium-catalyzed cross-coupling reactions. By using this bis(carbazol-9-yl)triphenylamine moiety as an end-cap, we are able to reduce the crystallization and retain the high-emission ability of these planar fluorescent oligoarylene cores in the solid state, as well as improve the amorphous stability and solubility of the materials. The results of optical and electrochemical studies show that their HOMOs, LUMOs, and energy gaps can be easily modified or fine-tuned by either varying the degree of π-conjugation or using electron affinities of the aryl cores which include fluorene, oligothiophenes, 2,1,3-benzothiadiazole, 4,7-diphenyl-4-yl-2,1,3-benzothiadiazole, and 4,7-dithien-2-yl-2,1,3-benzothiadiazole. As a result, their emission spectra measured in solution and thin films can cover the full UV−vis spectrum (426−644 nm). Remarkably, solution-processed nondoped BCPA-Ars-based OLEDs could show moderate to excellent device performance with emission colors spanning the whole visible spectrum (deep blue to red). Particularly, the RGB (red, green, blue) OLEDs exhibit good color purity close to the pure RGB colors. This report offers a practical approach for both decorating the highly efficient but planar fluorophores and tuning their emission colors to be suitable for applications in nondoped and solution-processable full-color emission OLEDs.
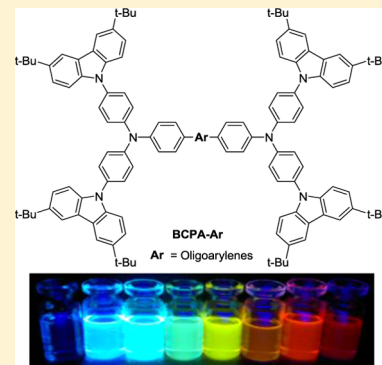
INTRODUCTION

Since the pioneering work on the first organic light-emitting diodes (OLEDs) by Tang in 1987,[1] OLEDs and displays made from these devices have received tremendous interest due to their excellent technological aspects such as low-cost, ease of fabrication using standard techniques (e.g., vacuum deposition or solution processing), the possibility of realizing flexible or large-area displays, and use in lighting applications.[2] In today's developments of OLED technologies, the trends of OLEDs are mainly focusing both on optimizations of device structures and developments of new emitting materials. In terms of the device fabrication, solution-processed OLEDs that are fabricated using small molecules will have great advantages because the materials that are used are easy to synthesize and purify, while the fabricating method is convenient, low-cost, and has large-scale manufacturability with less material usage.[3] The efficient tunability of the emission spectra of OLEDs to a desired color is an important consideration when designing materials. Obviously, the key point of materials development for full-color flat display is to determine materials emitting pure colors of red, green, and blue with excellent emission efficiency

and high stability; however, tuning emission color over the entire visible range has also emerged as an important ongoing research task.[4] A simple and efficient way to achieve full-emission color tuning OLEDs is to change the molecular structure of the emitting materials. Color tuning has been achieved in conjugated polymers and small molecules by systematic modification of the chemical structure of, for example, polythiophenes,[5] poly(*p*-phenylene vinylene) derivatives,[6] 1,6-bis(*N*-phenyl-*p*-(*R*)-phenylamino)pyrenes,[7] bis-dipolar diphenylamino-end-capped oligoarylfluorenes,[8] tris(5-aryl-8-quinolinolate)Al(III) complexes,[9] and iridium complexes.[10] However, the limitation of these materials is that their emission colors and the EL spectra of the OLEDs do not span the entire visible spectrum. In terms of material development, it is worthwhile to explore a new group of organic materials that can emit at wavelengths across the whole visible spectrum, while possessing similar physical properties and processability. In this paper, we report the design, synthesis, and light-emitting

properties of a group of novel bis(3,6-di-*tert*-butylcarbazol-9-ylphenyl)aniline end-capped oligoarylenes, BCPA-Ars (Scheme 1), in our aim to develop solution-processable small molecules

Scheme 1. Molecular Structures of a Series of Bis(3,6-di-*tert*-butylcarbazol-9-ylphenyl)aniline End-Capped Oligoarylenes (BCPA-Ars)
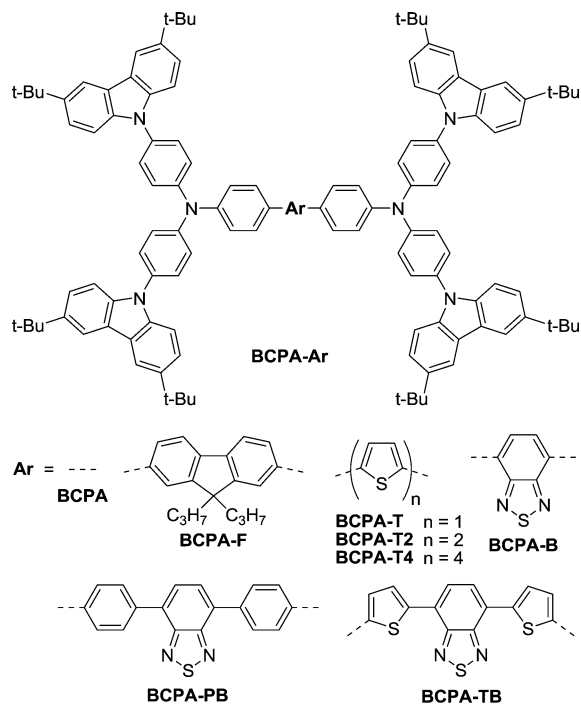

which are capable of acting as nondoped emitters to achieve efficient full-emission color tuning in OLEDs. The use of bis(carbazol-9-yl)triphenylamine moieties as end-capping groups aims to fulfill the following purposes: (1) to form nonplanar molecules for suppression of aggregation-induced fluorescence quenching of the planar conjugated core as well as improve solubility, thermal stability, and prevention of intermolecular interaction, (2) to increase the hole-transporting capability so as to make the target molecules suitable as nondoped emitters, and (3) to provide sufficient molecular weight and viscosity to make the products suitable for solution process. Many of the carbazole and triarylamine derivatives have been employed as excellent hole-transporting materials with superior amorphous and thermal stability.[11] The structural modifications of oligoarylene fluorescent cores by either varying the degree of π-conjugation or using the electron-withdrawing effect of the aryl cores such as fluorene, oligothiophenes, 2,1,3-benzothiadiazole, 4,7-diphenyl-4-yl-2,1,3-benzothiadiazole, and 4,7-dithien-2-yl-2,1,3-benzothiadiazole will allow the fine-tuning of the emission colors that cover the whole UV−vis spectrum. Using fluorene as a core will give a deep blue-emitting molecule,[12] while using oligothiophenes will extend the π-conjugation, and the molecules will emit in longer wavelengths (sky blue to yellow).[13] By employing a push−pull character of the donor feature of triarylamine end-caps and the acceptor nature of 2,1,3-benzothiadiazole core, combined with using either phenyl or thiophene spacers to control the push−pull extent, the molecules will emit in the long- wavelengths region (yellow to red). With this design, simple solution-processed hole-transporting nondoped emitters can be obtained, and

simple structure full-emission color tuning nondoped OLEDs can be fabricated. Nondoped OLEDs can avoid reproducibility problems associated with achieving the optimum doping concentration during processing and are easily adapted to a mass production line. Herein, we describe a detailed synthesis of BCPA-Ars including physical and photophysical properties. The investigation of a solution-processed OLED device fabrication and performance is also reported.

■ RESULTS AND DISCUSSION

Synthesis. The target BCPA-Ars were then synthesized by means of double palladium-catalyzed cross-coupling reactions of the iodo/bromo intermediates including 4-(5-bromothiophen-2-yl)-*N,N*-bis(4-(3,6-di-*tert*-butylcarbazol-9-yl)-phenyl)-4-iodoaniline (**1**), 4-(5-bromothiophen-2-yl)-*N,N*-bis-(4-(3,6-di-*tert*-butylcarbazol-9-yl)phenyl)aniline (**3**), 4-(5′-[2,2′-bithiophen]-5-yl)-*N,N*-bis(4-(3,6-di-*tert*-butyl carbazol-9-yl)phenyl)aniline (**5**), and 4-(4-bromophenyl)-*N,N*-bis(4-(3,6-di-*tert*-butylcarbazol-9-yl)phenyl)aniline (**6**), as outlined in Scheme 2. The bromo intermediates **3** and **5** were synthesized in good yields from **1** using a reaction sequence of Suzuki cross-coupling reaction with 2-thiophene boronic acid catalyzed by Pd(PPh$_3$)$_4$/Na$_2$CO$_3$ in THF and a bromination reaction with NBS in THF in an iterative manner. The cross-coupling of **1** with 4-bromophenylboronic acid gave **6** in 76% yield. Cross-coupling reactions of these iodo/bromo intermediates **1**, **3**, **5**, and **6** either with 2,1,3-benzothiadiazole-4,7-bis(boronic acid pinacol ester), 9,9-dipropylfluorene-2,7-bis(boronic acid pinacol ester), and 2,5-thiophenediboronic acid under Suzuki coupling conditions or with hexabutylditin under Stille coupling conditions were performed to afford the desired bis(carbazol-9-yl)triphenylamine end-capped oligoarylenes (BCPA-Ars) in moderate to good yields of 58−79%. Colors of the solid products were spread from colorless to dark red. All the newly synthesized BCPA-Ars were fully characterized with ^{1}H NMR, ^{13}C NMR, FTIR, and high-resolution mass spectrometry and were found to be in good agreement with the structures. These materials show high solubility in most organic solvents allowing their thin films to be fabricated by a spin-coating process. The morphology of their spin-cast films, which is another key factor for OLED fabrication, was investigated by atomic force microscopy (AFM). All thin films spin-coated from CHCl$_3$/toluene solution have a fairly smooth and pinhole-free surface, indicating that they have good film-forming properties and can be fabricated by low-cost solution processes (Figure 1 and Figure SI_1, Supporting Information).

Quantum Chemical Calculations. To understand the geometries and electronic properties of the BCPA-Ar series, quantum chemical calculations were performed using the TDDFT/B3LYP/6-31 G(d,p) method.[14] Their optimized structures reveal that the bis(carbazol-9-yl)triphenylamine moieties attached to the end of the molecules adopt a bulky conformation creating nonplanar geometry around the planar oligoarylene cores, which could help to prevent the close π−π contact between molecules and enhance their thermal properties.[15] In the HOMO of BCPA-Ars, π-electrons are delocalized over the entire oligoarylene core and end-capping moieties. In the LUMOs of BCPA-F and BCPA-T1−4, having fluorene and oligothiophenes as cores, respectively, the excited electrons delocalize over the quinoid-like fluorene and oligothiophene planes, while in the LUMOs of BCPA-B, BCPA-PB, and BCPA-TB, which have an electron-deficient 2,1,3-benzothiadiazole as a central aryl core, these electrons delocalize mainly on the

Scheme 2. Synthetic Route to Oligoarylenes BCPA-Ars[a]
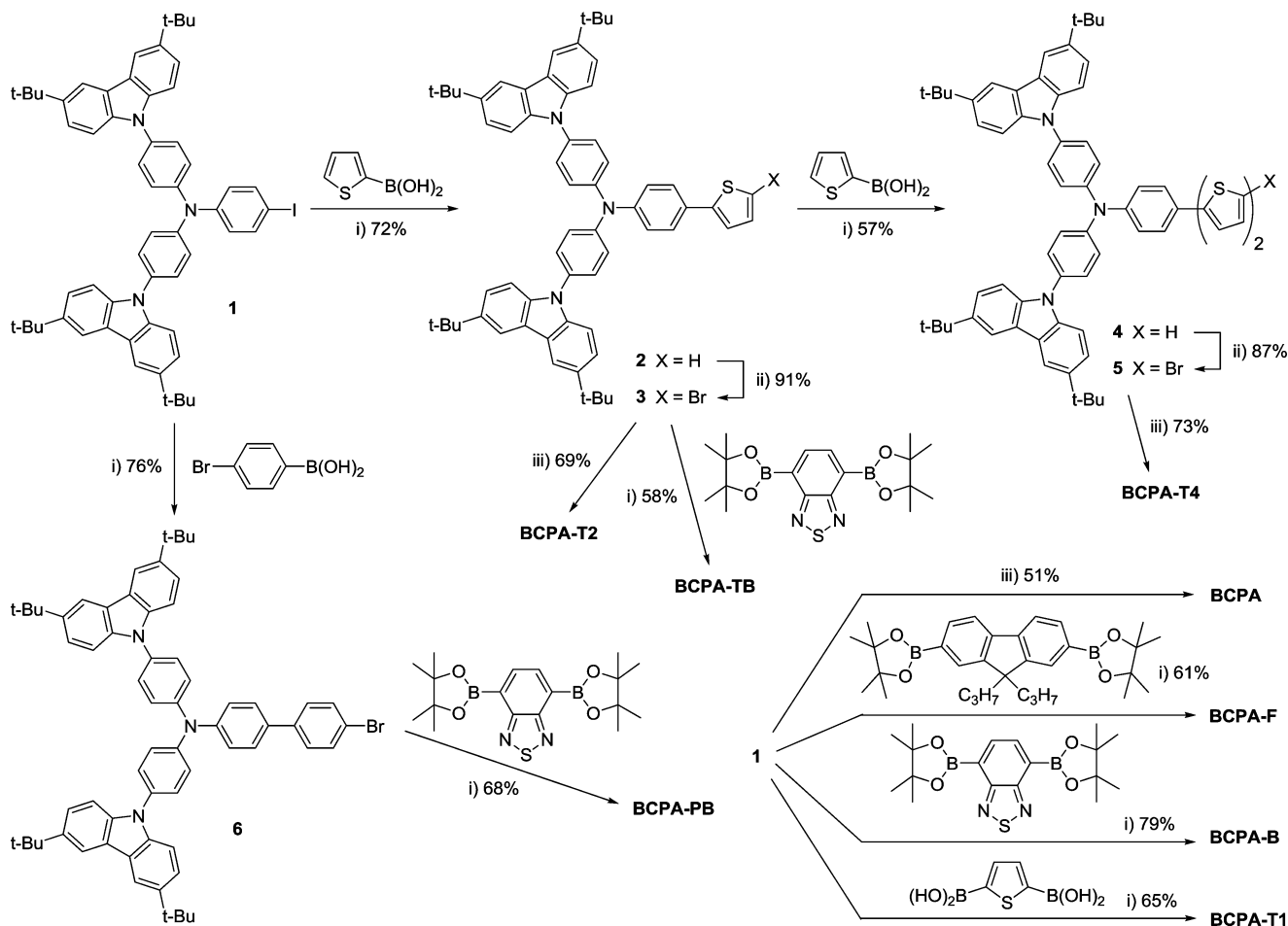
[a] (i) Pd(PPh₃)₄, 2 M Na₂CO₃,THF, heat; (ii) NBS, THF; (iii) (Bu)₃Sn−Sn(Bu)₃, Pd(PPh₃)₄, toluene, heat.
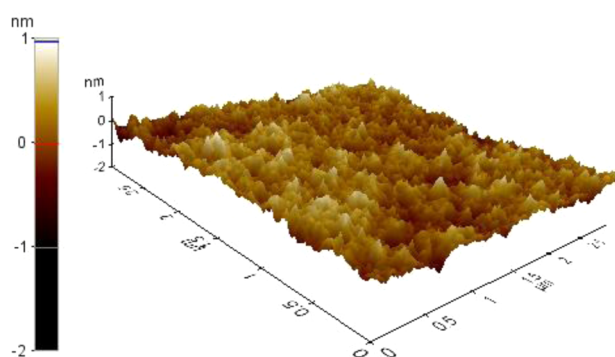

Figure 1. AFM image of the spin-coated film of BCPA-B.

quinoid-like 2,1,3-benzothiadiazole plane, creating a donor−acceptor characteristic (Figure 2 and Figure SI_2, Supporting Information). The HOMO−LUMO energy gaps (E_g cal) of BCPA-Ars were calculated and are summarized in Table 1. These E_g cal values (1.78−3.21 eV) are slightly deviated from those estimated from the absorption onset (2.02−3.13 eV). There are factors responsible for the errors in the calculated results because the orbital energy difference between HOMO and LUMO is still an approximate estimation of the transition energy because the transition energy also contains significant contributions from two-electron integrals. The real situation is that an accurate description of the lowest singlet excited-state

requires a linear combination of a number of excited configurations.

Photophysical Properties. Optical properties of the BCPA-Ar series were investigated in CH_2Cl_2 solution and thin films spin-coated on quartz substrates. The pertinent data are summarized in Table 1. The solution UV−vis absorption spectra of BCPA-Ars exhibit two common absorption bands at 298 nm that assigns to the π−π* electron transition of the peripheral carbazole moieties, and 332−349 nm that is consistent with the π−π* electron transition of the bis-(carbazol-9-yl)triphenylamine end-caps (Figure 3a). The spectra of BCPA-F and BCPA-T1−4 reveal that the extra absorption bands at longer wavelengths (373−450 nm) are assigned to the π−π* electron transition of their corresponding fluorene and oligothiophenes cores. These bands are gradually red-shifted from 373 to 450 nm with the increasing number of thiophene rings indicating an extended π-conjugated molecule, as expected. However, the absorption bands of BCPA-B, BCPA-PB, and BCPA-TB are shifted to longer wavelengths (422−528 nm) and belong to an intramolecular charge-transfer (ICT) transition from the donor (end-capping groups) to the acceptor (2,1,3-benzothiadiazole core). The solution photo-luminescence (PL) spectra of BCPA-Ars exhibit featureless emission bands covering the entire UV−vis spectrum (422−640 nm), and upon illumination, the emission colors display a range from deep blue to red (Figure 3b). This indicates that by
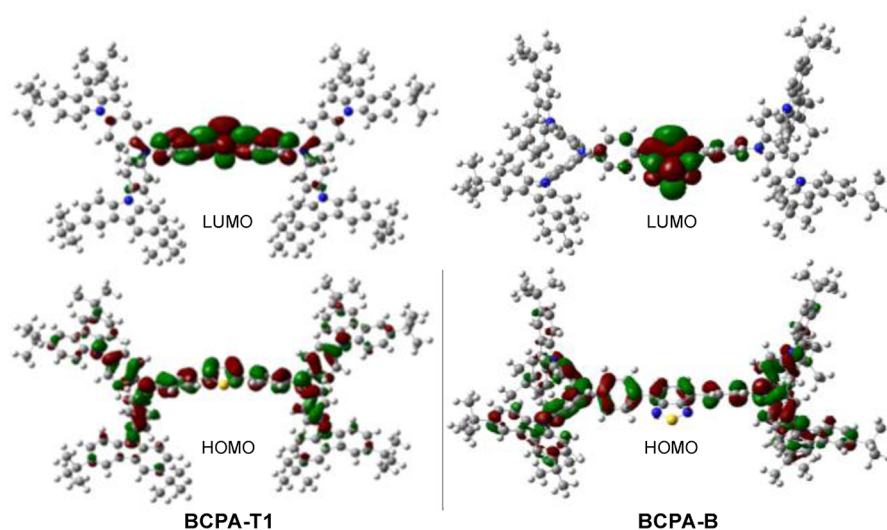
Figure 2. HOMO and LUMO orbitals of BCPA-T1 and BCPA-B calculated by the TDDFT/B3LYP/6-31G(d,p) method.

Table 1. Physical Data of Oligoarylenes BCPA-Ars

comp	λ_{abs} (log ε)[a] (nm, M^{-1} cm^{-1})	λ_{em}[a] (nm)	λ_{em}[b] (nm)	Φ_F[a]	Stokes shift[c] (nm)	$T_g/T_m/T_{5d}$[d] (°C)	$E_{1/2}$ vs Ag/Ag$^+$[e] (V)	E_{onset}^{ox}[e] (V)	E_g[f] (eV)	E_g cal[g] (eV)	HOMO/LUMO[h] (eV)
BCPA	349 (5.00)	422	426	0.55	73	223/ - /326	0.73, 0.85, 1.11, 1.45	0.69	3.13	3.21	−5.13/−2.00
BCPA-F	373 (4.64)	443	444	0.71	70	234/ - /358	0.80, 1.11, 1.40, 1.67	0.73	2.99	3.04	−5.17/−2.18
BCPA-T1	396 (4.74)	465	488	0.65	69	242/ - /333	0.74, 0.82, 1.15, 1.40	0.68	2.77	2.79	−5.12/−2.35
BCPA-T2	418 (4.85)	494	517	0.24	76	241/324/344	0.74, 1.13, 1.33, 1.55	0.66	2.58	2.55	−5.10/−2.52
BCPA-T4	450 (4.93)	529	545	0.14	79	247/372/378	0.66, 0.77, 0.94, 1.12, 1.21, 1.26, 1.45, 1.59	0.63	2.39	2.25	−5.07/−2.68
BCPA-B	462 (4.40)	600	601	0.05	138	243/343/330	0.82, 1.11, 1.45	0.76	2.32	2.06	−5.20/−2.88
BCPA-PB	422 (4.32)	513	528	0.03	91	243/363/368	0.80, 1.11, 1.43, 1.73	0.76	2.53	2.16	−5.20/−2.67
BCPA-TB	528 (4.33)	640	644	0.08	112	255/368/339	0.74, 0.80, 1.08, 1.29, 1.48	0.72	2.02	1.78	−5.16/−3.14

[a]Measured in CH$_2$Cl$_2$. [b]Measured in thin film spin-coated on quartz substrate. [c]Calculated from the difference of λ_{max}^{abs} and λ_{max}^{em}. [d]Measured by DSC/TGA at a heating rate of 10 °C min^{-1}. [e]Obtained from CV and DPV at a scan rate of 50 mV·s^{-1} in CH$_2$Cl$_2$ and n-Bu$_4$NPF$_6$ as the electrolyte. [f]Estimated from the optical absorption edge, $E_g = 1240/\lambda_{onset}$. [g]Obtained from quantum calculation using TDDFT/B3LYP/6-31G(d,p). [h]Calculated by HOMO = −(4.44 + E_{onset}^{ox}), and LUMO = HOMO − E_g, where E_{onset}^{ox} is the onset potential of the oxidation.

using different π-extended and electron-affinitive aryl cores, the fine-tuning of the optical properties of molecular materials can be achieved. Generally, with a longer π-conjugation length or stronger electron-withdrawing strength of the central core, there is a longer emission-wavelength shift. Moreover, the fluorescence spectra are excitation-wavelength-independent, and because of excitation at either bis(carbazol-9-yl)-triphenylamine end-caps or oligoarylene cores, the emission spectra are identical. This suggests that energy or excitation can be efficiently transferred from the triarylamine moieties to the emissive oligoarylene cores, as observed in the quantum calculation. The fluorescence spectra of BCPA-B, BCPA-PB, and BCPA-TB are solvent-dependent, in which the spectra exhibit red-shifts with an increase in solvent polarity. For instance, the emission maxima of BCPA-TB, BCPA-B, and BCPA-PB exhibit a solvatochromatic shift of 50, 47, and 40 nm, respectively, changing from cyclohexane to DMSO (Figure 3c). This suggests that the emission excited states of these 2,1,3-benzothiadiazole derivatives possess charge-transfer character. BCPA, BCPA-F, and BCPA-T1−4 show small Stokes shifts (69−79 nm), while BCPA-B, BCPA-PB, and BCPA-TB exhibit large Stokes shifts (91−138 nm) in solution, which are typically

associated with compounds that have strong ICT character. The fluorescence quantum yields (Φ_F) of BCPA-Ar series that were measured in CH$_2$Cl$_2$ using quinine sulfate or coumarin 6 as a standard are in the range of 0.03−0.71 (Table 1). In this series, BCPA-F has the highest Φ_F value of 0.71 due to the better chromophore of the fluorene core. In contrast, the donor−acceptor character of BCPA-B, BCPA-PB, and BCPA-TB accounts for their low Φ_F (0.03−0.08) due to fluorescence quenching by electron exchange according to the Dexter mechanism.[16] The Φ_F values of BCPA-T1−4 (0.14−0.65) are found to decrease with the increasing number of thiophene units, which is commonly observed in most cases of oligothiophene derivatives.[17] Due to the long oligothiophenes, the molecules will become extended planar structures and will be prone to fluorescence quenching brought about by $\pi\pi$ stacking interactions of the oligomer segments. However, these materials show good fluorescence in the solid state. The thin film photoluminescence (PL) spectra of BCPA-Ar series also show featureless emission bands and exhibit a small to moderate red shift ($\approx$1−23 nm) in emission maxima as compared to those obtained from dichloromethane (Figure 3d). This suggests that the bulky molecular structure of end-
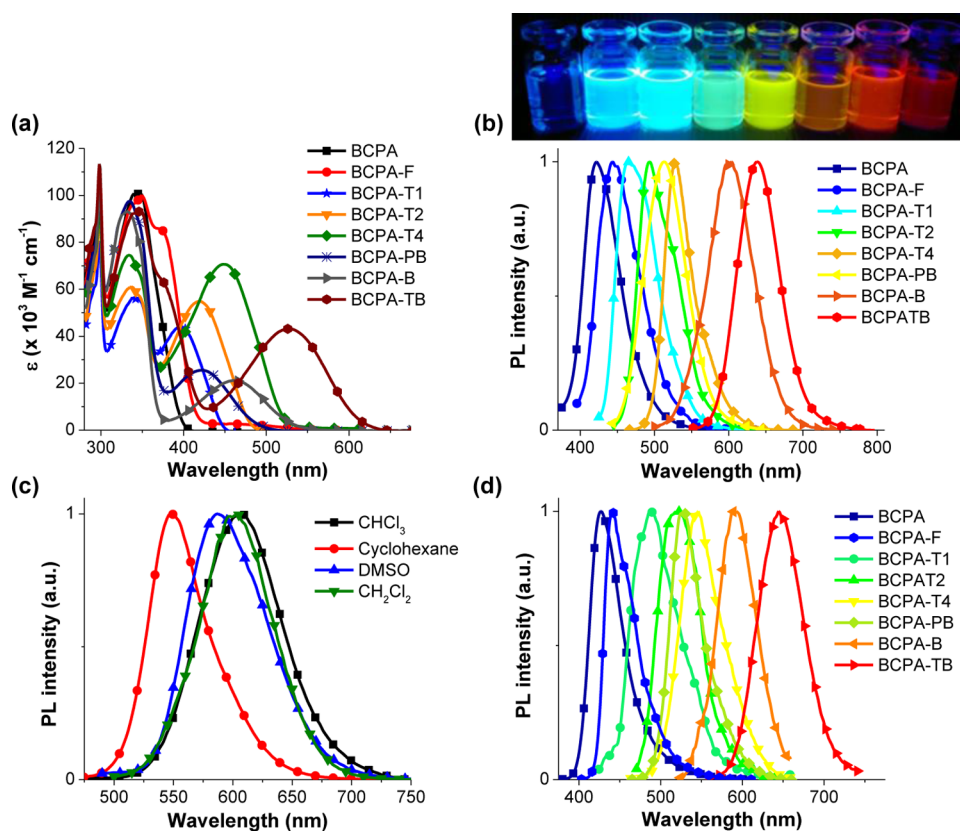
Figure 3. (a) Absorption spectra of BCPA-Ars measured in CH_2Cl_2. (b) PL spectra of BCPA-Ars in CH_2Cl_2 and their emission colors upon illumination. (c) PL spectra of BCPA-B in different solvents. (d) PL spectra of BCPA-Ars in thin films spin-coated on quartz substrates.

capping groups prevents the intermolecular $\pi-\pi$ interactions of the fluorescent core in the solid state. The most apparent difference in emission spectra comes from those bearing oligothiophene as a central core in which the red shift is attributed to the improvement in the coplanarity of the thienyl moieties in the solid state. Importantly, the emission spectra of the thin film PL of BCPA-Ars also cover the full visible spectrum.

Electrochemical and Thermal Properties. To analyze the redox properties of these bis(carbazol-9-yl)triphenylamine end-capped oligoarylenes, cyclic voltammetry (CV) and differential pulse voltammetry (DPV) were performed in a three-electrode cell setup with 0.1 M Bu_4NPF_6 as a supporting electrolyte in CH_2Cl_2. The results are tabulated in Table 1. DPV and CV curves of the BCPA-Ar series exhibit well-defined multiple quasi-reversible oxidation waves (Figure 4 and Figure SI_3, Supporting Information). Under this experimental condition, no reduction is observed in all cases. The first oxidation wave is assigned to the removal of electrons from the peripheral carbazoles, resulting in radical cations. Their multiple CV scans reveal identical CV curves with no additional peak at a lower potential on the cathodic scan (E_{pc}), suggesting that no electrochemical coupling at the 3,6-positions of the carbazole peripheries occurs as they are protected by *tert*-butyl groups, indicating electrochemically stable molecules, as expected (Figure SI_4, Supporting Information).[18] It was determined that, in cases of BCPA-F and BCPA-T1−4, the first oxidation potentials gradually shift to lower potentials with increasing size of the π-conjugation system, and this finding agrees with the optical results. Similar behavior has also been observed in other end-capped oligothiophenes.[19] The HOMO and LUMO
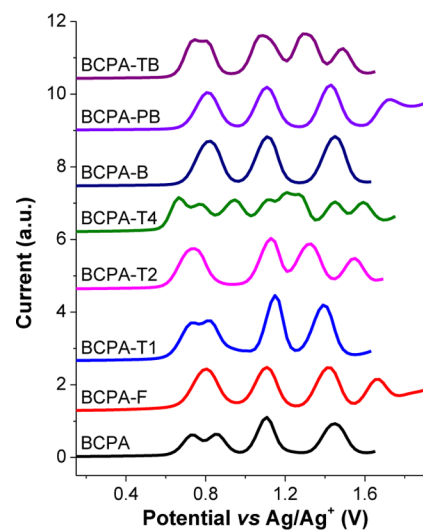

Figure 4. Traces of differential pulse voltammetric measurements of BCPA-Ars at a scan rate of 50 mV s^{-1}.

energy levels of BCPA-Ars are calculated from the oxidation onset potentials (E_{onset}^{ox}) and energy gaps (E_g), and the results are listed in Table 1. The HOMO energy levels of these materials are in the range of −5.07 to −5.20 eV, matching well with the work function of the indium tin oxide (ITO) electrode and favoring the injection and transport of holes. Their LUMO energy levels vary widely with a range of −2.00 to −3.14 eV. Because of the electron-withdrawing nature of the aryl central cores, the LUMOs of BCPA-Ar are stabilized in various degrees as compared to that of BCPA (LUMO = −2.00 eV), which has

no aryl core. The LUMOs of BCPA-B, BCPA-PB, and BCPA-TB (-2.67 to -3.14 eV) having an electron-poor 2,1,3-benzothiadiazole as a central aryl core are lower and closer to the work function of the LiF/Al anode than those of BCPA-F and BCPA-T1$-$4 (-2.00 to -2.68 eV). Consistently, the stronger the electron-withdrawing strength, the more stabilized the LUMO. These results further support that the LUMOs, HOMOs, and energy gaps of these oligoarylenes can be easily modified or tuned by the use of different π-extended and electron-affinitive aryl cores.

The thermal properties of these oligoarylenes were analyzed by differential scanning calorimetry (DSC) and thermogravimetric analysis (TGA) (Table 1, Figure SI_5, Supporting Information). With the incorporation of bis(3,6-di-*tert*-butyl-carbazol-9-ylphenyl)aniline as the end-caps, all the newly synthesized BCPA-Ar series exhibit an exceptionally high glass transition temperature (T_g) in the range of 223$-$255 °C, indicating that they have the ability to form a morphologically stable amorphous thin film. They also show high thermal stabilities with a decomposition temperature at 5% weight loss (T_{5d}) at a temperature well over 326 °C (Figure SI_5, Supporting Information). The T_g values of BCPA-T1$-$4, for example, are higher than those of triarylamine end-capped oligothiophenes (T_g = 90$-$98 °C)[20] and triarylamine-substituted carbazole-based dendritic oligothiophenes (T_g = 139$-$196 °C).[21] These results prove that the use of bis(carbazol-9-yl)triphenylamine as end-capping groups could reduce the crystallization of a planar-conjugated core and improve the amorphous stability of the material and the thin film, which in turn could increase the service time in device operation.[22]

Electroluminescence Properties. According to the above-discussed excellent properties including low first ionization potential, good luminescence properties, high thermal stability, good amorphous morphological stability, and ability to form good thin film from the solution spin-coating process, BCPA-Ars show great potential for use as solution-processed nondoped hole-transport emitters in OLEDs. First, single-layer devices with the structure of ITO/PEDOT:PSS/BCPA-Ars(spin-coating)/LiF(0.5 nm):Al(150 nm) were fabricated and investigated. The BCPA-Ar layer was spin-coated from a CHCl$_3$/toluene (5:1) solution with controlled thickness. The electroluminescent characteristics of the devices are shown in Figure 5 and summarized in Table 2. It is found that only the devices using BCPA-T4 (device I), BCPA-B (device II), BCPA-PB (device III), and BCPA-TB (device IV) as an emitting layer (EML) show light emission. Analysis of the energy-band diagram of all fabricated single-layer devices reveals that the LUMO energy levels of BPPA, BCPA-F, and BCPA-T1$-$2 are too high and mismatch with the work function of the LiF/Al (4.20 eV) cathode with the electron injection barriers at the EML/LiF/Al interface as high as 2.17$-$2.20 eV (Figure 6a). The results reveal that the ICT effect and the favorable contributions are so well-balanced in 2,1,3-benzothiadiazole-based molecules (BCPA-B, BCPA-PB, and BCPA-TB) that they produce the best light-emission performance in single-layer OLEDs among all these analogues. The EL spectra of these devices (I$-$IV) exhibit a featureless emission peak matching well with the PL spectra of thin films indicating that the EL originates purely from the oligoarylenes (Figure 5b). The devices (II$-$IV) using BCPA-B, BCPA-P, and BCPA-TB as EML exhibit good to excellent device performance with maximum luminance (L_{max}) of 4523$-$7851 cd m^{-2}
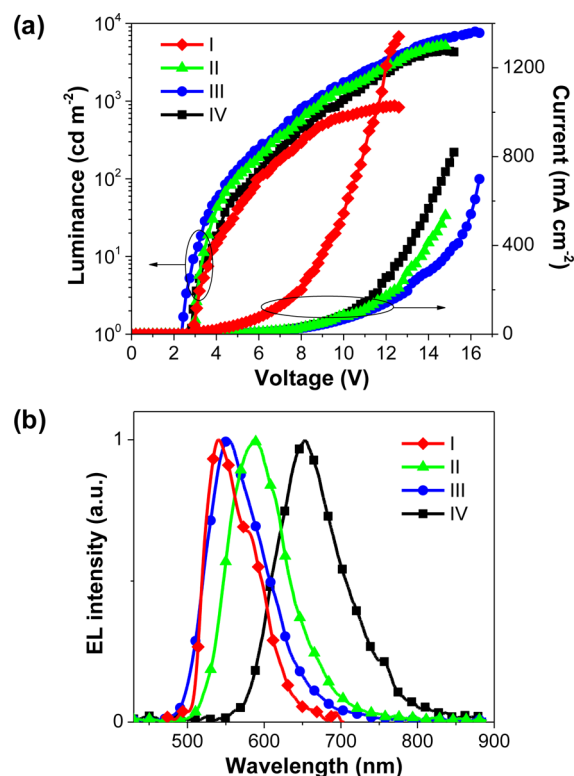
Figure 5. Plots of (a) current density$-$luminance$-$voltage and (b) EL spectra of the single-layer OLEDs (devices I$-$IV).

and luminance efficiencies (η_{max}) up to 1.53$-$3.85 cd A^{-1} (Figures SI_6, Supporting Information). Particularly, the BCPA-TB-based single-layer device (IV) emits a bright red luminescence with excellent color purity, an emission peak at 652 nm, and a full width at half-maximum of $\approx$ 100 nm. The coordinates of the emitted light specified by the Commission Internationale De L'Eclairage (CIE) are x = 0.65 and y = 0.33, which are very close to the pure red color (x = 0.67, y = 0.33) standardized by the National Television System Committee (NTSC).[23] This device emits better red color purity and has less complex device structure than those of the devices featuring 1,10-dicyano-substituted bis-styrylnaphthalene derivative (BSN),[24] (bis(4-(N-(1-naphthyl)phenylamino)phenyl)-fumaronitrile) (NPAFN),[25] or a star-shaped thieno-3,4-b-pyrazine (TPNA)[26] as the nondoped materials. This solution-processed single-layer red OLED (device IV) shows an L_{max} of 4523 cd m^{-2} at 14.8 V, η_{max} of 1.53 cd A^{-1}, and turn-on voltage (V_{on}) of 2.9 V. The BCPA-PB-based device (III) gives a yellow emission with a peak maximum (λ_{em}) at 553 nm, a high efficiency (L_{max} = 7851 cd m^{-2} at 14.8 V, η_{max} = 3.85 cd A^{-1}), and a low V_{on} of 2.4 V, while the BCPA-B-based device (II) emits a bright orange color (λ_{em} = 586 nm) with a slightly lower efficiency (η_{max} = 2.46 cd A^{-1}).

To improve the efficiency of the single-layer OLED and achieve light emission from BPPA, BCPA-F and BCPA-T1$-$2, a multilayer device is necessary. This could be done by balancing a charge injection in the device. In this case, BCPA-Ars are more hole-injection EML as their HOMOs (-5.07 to -5.20 eV) match well with the work function of the ITO/PEDOT:PSS anode (-5.00 eV), hence an electron-injection/hole-blocking layer is required (Figure 6a). Dimethyl-4,7-diphenyl-1,10-phenanthroline (BCP) is known to enhance performance in multilayer devices fabricated with predom-

Table 2. Electroluminescent Data of the Single-Layer OLEDs

device[a]	EML	λ_{max}EL (nm)	V_{on}/V_{100}[b] (V)	L_{max}/V[c] (cd m^{-2}, V)	J_{max}[d] (mA cm^{-2})	η_{max}[e] (cd A^{-1})	CIE (x, y)
I	BCPA-T4	540	2.9/5.9	873/12.4	1307	0.16	0.39, 0.55
II	BCPA-B	586	2.9/4.9	5212/14.6	456	2.46	0.52, 0.46
III	BCPA-PB	553	2.4/4.7	7851/16.2	607	3.85	0.43, 0.55
IV	BCPA-TB	625	2.7/5.7	4523/14.8	732	1.53	0.65, 0.33

[a]ITO/PEDOT:PSS/EML/LiF:Al. [b]Turn-on voltages at 1 and 100 cd m^{-2}. [c]Maximum luminance at applied voltage. [d]Current density at maximum luminance. [e]Luminance efficiency.
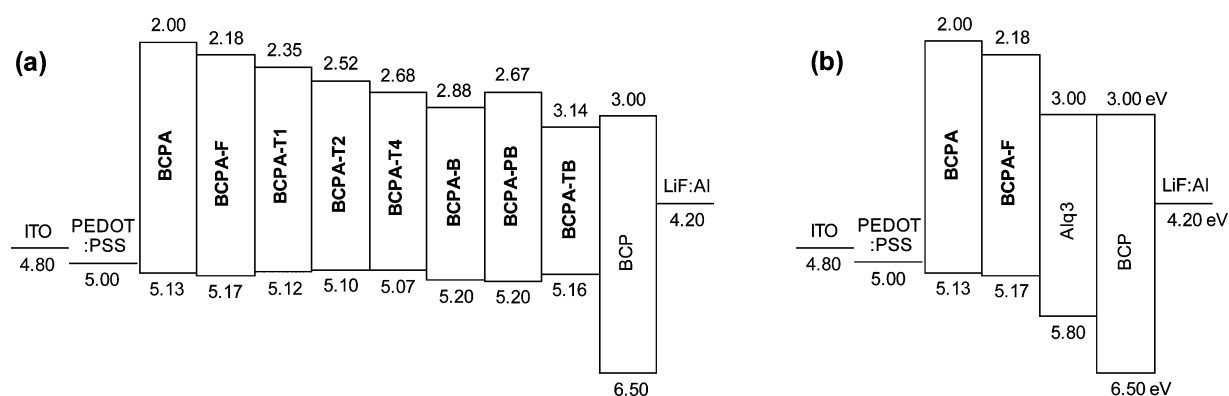

Figure 6. Schematic energy diagrams of the fabricated OLEDs using (a) BCPA-Ars as EML and (b) BCPA and BCPA-F as HTL.
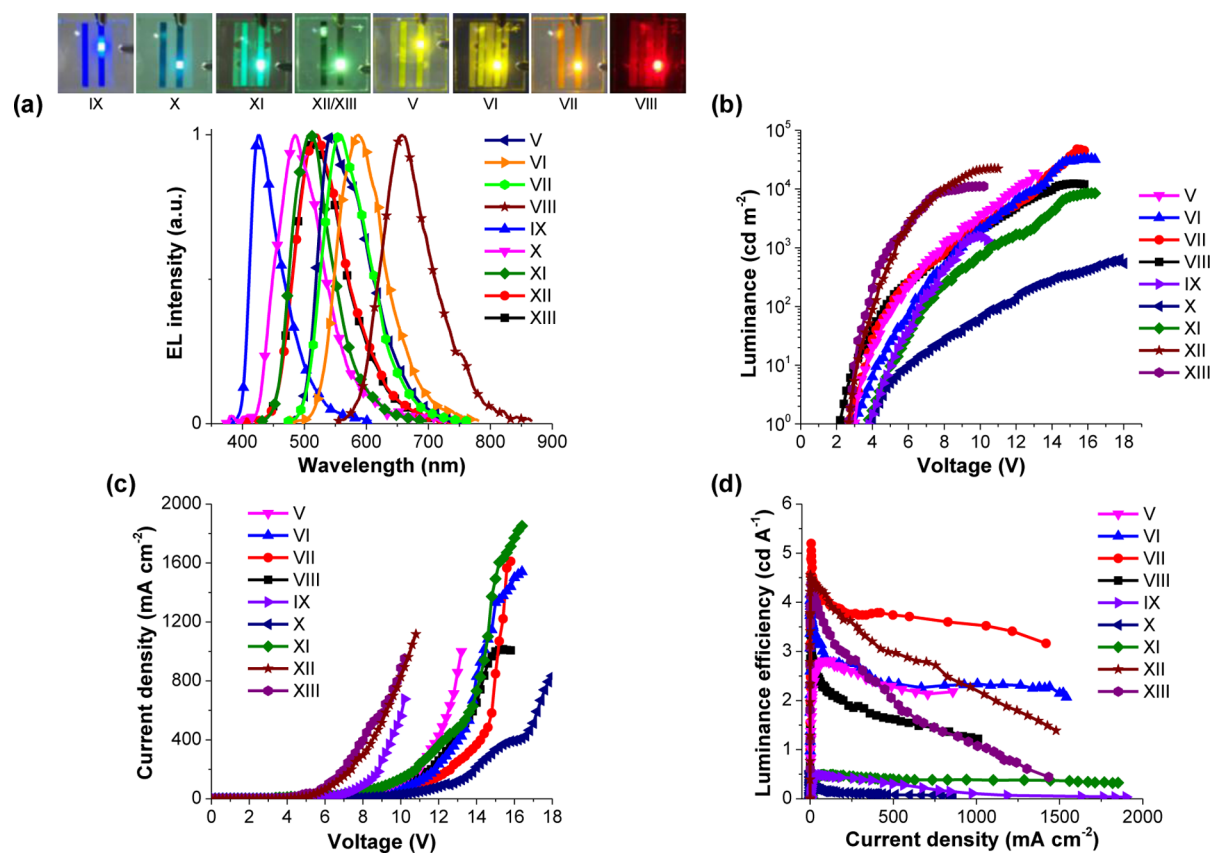

Figure 7. Plots of (a) EL spectra and emission colors, (b) luminance−voltage, (c) current density−voltage, and (d) efficiency−current density of the double-layer OLEDs (device V−XIII).

inantly hole-transporting emitters.[27] Simple double-layer devices with the structure of ITO/PEDOT:PSS/BCPA-Ars-(spin-coating)/BCP(40 nm)/LiF(0.5 nm)/Al(150 nm) were fabricated and investigated. The detailed EL and *J*−*V*−*L* data are shown in Figure 7 and summarized in Table 3. The spin-

coated double-layer OLEDs using BCPA-T4 (device V), BCPA-B (device VI), BCPA-PB (device VII), and BCPA-TB (device VIII) as EML exhibit a massive improvement in the device performance compared to their single-layer devices with an L_{max} of 12325−47497 cd m^{-2} and η_{max} up to 2.18−5.19 cd

Table 3. Electroluminescent Data of the Double-Layer OLEDs

device	EML/HTL	λ_{max}EL (nm)	$V_{on}/V_{100}{}^c$ (V)	L_{max}/V^d (cd m^{-2}, V)	$J_{max}{}^e$ (mA cm^{-2})	$\eta_{max}{}^f$ (cd A^{-1})	CIE (x, y)
V[a]	BCPA-T4	542	3.0/5.1	18699/13.0	858	2.81	0.43, 0.55
VI[a]	BCPA-B	587	2.7/5.0	47497/15.4	1221	5.19	0.53, 0.46
VII[a]	BCPA-PB	557	2.9/6.2	32817/15.8	1440	4.17	0.44, 0.54
VIII[a]	BCPA-TB	653	2.2/4.7	12325/15.2	1009	3.97	0.66, 0.33
IX[a]	BCPA-F	426	4.0/6.7	1572/10.0	561	0.49	0.16, 0.08
X[a]	BCPA-T1	484	4.0/10.8	640/17.8	764	0.57	0.19, 0.33
XI[a]	BCPA-T2	510	3.7/6.9	8489/16.0	1768	0.49	0.22, 0.52
XII[b]	BCPA-F	521	2.4/4.1	22238/10.6	1046	4.55	0.29, 0.53
XIII[b]	BCPA	520	2.5/3.8	11275/10.0	888	4.37	0.29, 0.53
XIV[b]		518	4.2/5.4	4961/10.0	693	0.91	0.30, 0.54
XV[b]	TPD	519	2.5/3.7	22539/8.8	1296	4.05	0.29, 0.53

[a]ITO/PEDOT:PSS/EML/BCP/LiF:Al. [b]ITO/PEDOT:PSS/HTL/Alq$_3$/LiF:Al. [c]Turn-on voltages at 1 and 100 cd m^{-2}. [d]Maximum luminance at applied voltage. [e]Current density at maximum luminance. [f]Luminance efficiency.

A^{-1}. The colorimetric purities of these double-layer devices are also equivalent to their single-layer devices. The double-layer OLEDs fabricated with BCPA-F (device IX) and BCPA-T1−2 (devices X and XI) as EML show moderate device performance. These devices exhibit an L_{max} of 640−8489 cd m^{-2} and η_{max} up to 0.49−0.57 cd A^{-1}. The EL spectra of all devices (V−XI) exhibit a featureless emission peak identical to their PL spectra of thin films and also their single-layer OLED devices, indicating that they have similar relaxation processes (Figure 7a). Furthermore, no emission shoulder is detected at a longer wavelength, which often occurs in devices fabricated from EMLs with planar molecular structure due to excimer and exciplex species formation at the interface of the EML and BCP layers.[28] Moreover, stable emission is obtained from all devices, and the EL spectra did not change over the entire driven voltages (Figure SI_7, Supporting Information). Unfortunately, there is still not sufficient light emission from the BCPA-based double-layer OLED. This may be the result of a higher LUMO level of BCPA than is effective when used as EML. However, the electroluminescence (EL) spectra of these BCPA-Ars-based devices (V−XI) do cover the entire visible spectrum with emission peaks ranging from 426 nm for the BCPA-F-based device to 653 nm for the BCPA-TB-based device. The role of the incorporated BPC layer into the BCPA-B- and BCPA-TB-based double-layer devices (VI, VIII) is preferably a hole-blocking layer as the LUMO of BCP (−3.00 eV) is similar to that of both BCPA-B and BCPA-TB, while in other devices (V, VII, IX−XI) BCP would act as both hole-blocking and electron-transporting layers (Figure 6a). In these BCPA-Ar series, the devices (VI, VII) fabricated with BCPA-B (orange emission) and BCPA-PB (yellow emission) as EML have the best performance in terms of L_{max} (32817−47497 cd m^{-2}) and η_{max} (4.17−5.19 cd A^{-1}), while the BCPA-TB-based spin-coating double-layer device (VIII) exhibits slightly lower performance (L_{max} = 12325 cd m^{-2}, η_{max} = 3.97 cd A^{-1}) with excellent red color purity (CIE = 0.66, 0.33) and low device turn-on voltage (V_{on}) of 2.2 V, which is considered to be one of the lowest turn-on voltages for solution-processed red OLEDs reported so far.[29] As far as we know, the ability of BCPA-TB as a nondoped red EML in red OLEDs, in terms of device performance, solution processability, thermal property, red color purity, and simple device structure, is outstanding compared with those solution-processable red fluorescent emitters[30] and is also comparable with vacuum-deposited red fluorescent emitters reported in recent years.[31] Noticeably, the BCPA-F-based double-layer device (IX) also emits an excellent deep blue color

(λ_{em} = 426 nm) with CIE coordinates of (0.16, 0.08), which is close to the NTSC standard deep blue (0.14, 0.08),[32] while the green OLED of the BCPA-T2-based device (XI) shows the λ_{em} around 510 nm with the CIE coordinates of (0.22, 0.52), which is slightly deviated from the NTSC standard green (0.26, 0.65).[33] The high EL efficiencies, high color purity, and facilitating process for the light-emitting films indicate these materials to be promising candidates for full-color-display applications, especially BCPA-TB for red and BCPA-F for deep blue.

As mentioned above, the simple structure OLEDs using BCPA as EML did not give light emission; however, its HOMO level (−5.13 eV) matched well with the work function of ITO (4.8 eV) with high LUMO level, and BCPA may potentially serve as an amorphous hole-transporting material (AHTM) with superior thermal property. To test this hypothesis, double-layer Alq$_3$-based green OLEDs with the structure of ITO/PEDOT:PSS/BCPA and BCPA-F (spin-coating)/Alq$_3$(50 nm)/LiF(0.5 nm):Al(150 nm) were fabricated and investigated, where BCPA and BCPA-F were used as hole-transporting layers (HTL) and tris(8-hydroxyquinoline)-aluminum (Alq$_3$) as the green light-emitting (EML) and electron-transporting layers (ETL). The reference devices (devices XIV and XV) fabricated with and without a commercial HTM, N,N′-bis(3-methylphenyl)-N,N′-bis-(phenyl)benzidine (TPD), as HTL were made for comparison. The detailed EL and J−V−L data are shown in Figure 7 and summarized in Table 3. The BCPA-F-based device (XII) exhibits excellent performance with a high L_{max} of 22238 cd m^{-2} for green OLED at 10.6 V, a low V_{on} of 2.4 V, and η_{max} of 4.55 cd A^{-1}. The operating voltage at 100 cd m^{-2} is as low as 4.1 V. The BCPA-based device (XIII) displays slightly lower performance in terms of a maximum brightness, turn-on voltage, and maximum luminance efficiency. Both devices XII and XIII emit a bright green luminescence (λ_{em} = 520 nm, CIE coordinates of (0.29, 0.53)) under applied voltage. The EL spectra match well with the PL spectrum of Alq$_3$, the EL of the reference devices (XIV and XV), and other reported devices.[11,34] No emission at longer wavelengths indicating the formation of exciplex species at the interface is detected. From these results, and in view of the fact that a barrier for electron migration at the Alq$_3$/HTL interface (≈0.9 eV) is higher than that for hole migration at the HTL/Alq$_3$ interface (≈0.6 eV) (Figure 6b), both BCPA and BCPA-F will act only as HTL, and Alq$_3$ will act preferably as an electron blocker more than as a hole blocker and charge recombination thus is confined to the

Alq$_3$ layer. More importantly, a stable emission is obtained from these diodes in which the EL spectra and CIE coordinates did not change over the entire applied voltages (Figure SI_7, Supporting Information). When devices are compared for the performance of both devices (XII and XIII) with the reference device (XIV), it is found that the incorporation of either BCPA or BCPA-F in the device as an HTL not only increases the η_{max} from 0.91 to 4.37–4.55 cd A^{-1} but also significantly decreases the V_{on} from 4.2 to 2.4–2.5 V, indicating an excellent AHTM ability of both materials. Moreover, the abilities as solution-processed AHTM of BCPA and BCPA-F in terms of thermal stability of amorphous film and their device luminance efficiencies are also greater than commonly used TPD (T_g = 63 °C) (device XV).

■ CONCLUSION

In summary, we demonstrated the design strategy and synthesis of BCPA-Ars as nondoped solution-processed light emitters for full-emission color tuning OLEDs. By varying the degree of π-conjugation or using the electron affinities of the aryl cores, their HOMOs, LUMOs, and energy gaps can be easily modified or tuned. Their emission spectra in solution and thin film span the entire visible light spectrum (422–640 nm), and the emission colors range from deep blue to red upon illumination. By using bis(3,6-di-*tert*-butylcarbazol-9-ylphenyl)aniline as end-capping groups, we are able to reduce the crystallization and retain the high-emissive ability of a planar fluorescent core in the solid state, as well as improve the amorphous stability and solubility of the materials. All of these materials can form morphologically stable amorphous thin films with T_g as high as 223–255 °C. The ICT effect and the favorable contributions are so well-balanced in 2,1,3-benzothiadiazole-based molecules that they produce a high light-emission performance in solution-processed nondoped single-layer OLEDs among all these analogues. The single-layer OLED with a luminance efficiency as high as 3.85 cd A^{-1} and a low turn-on voltage of 2.4 V is achieved. The solution-processed nondoped BCPA-Ars-based double-layer OLEDs exhibit moderate to excellent device performance with emission colors spanning the whole visible spectrum (deep blue to red). The RGB (red, green, blue) OLEDs based on these materials by a simple solution process exhibit moderate to high luminescence efficiency and good color purity close to the pure RGB colors. Especially, double-layer red and blue OLEDs show an excellent red color (λ_{em} = 653 nm) with CIE coordinates of (0.66, 0.33) and an excellent deep blue color (λ_{em} = 426 nm) with CIE coordinates of (0.16, 0.08), which are close to the NTSC standard red (0.67, 0.33) and standard deep blue (0.14, 0.08), respectively. The ability of BCPA-TB as a nondoped red light emitter, in terms of device performance, is excellent compared with those solution-processable red fluorescent materials and also equivalent to the vacuum-deposited red fluorescent materials reported in recent years. This report offers a useful strategy to adorn the highly efficient but planar fluorophore to be suitable for applications in solution-processable and nondoped OLEDs.

■ EXPERIMENTAL SECTION

Synthesis and Characterization. The reagents (chemicals) were purchased and used without further purification. All ^{1}H and ^{13}C NMR spectra were recorded using CDCl$_3$ as the solvent. Infrared (IR) spectra were measured as KBr disc. High-resolution mass spectra (micrOTOF) were obtained with electrospray and matrix-assisted laser

desorption ionization (ESI) and measured in the MALDI-TOF/TOF mode.

***N,N*-Bis(4-(3,6-di-*tert*-butylcarbazol-9-yl)phenyl)-4-iodoaniline (1).** A mixture of tris(4-iodophenyl)amine (3.0 g, 4.8 mmol), 3,6-di-*tert*-butylcarbazole (2.7 g, 9.6 mmol), CuI (0.9 g, 4.8 mmol), K$_3$PO$_4$ (3.3 g, 24.1 mmol), and ±-*trans*-1,2-diaminocyclohexane (0.6 mL, 4.8 mmol) in toluene (60 mL) was degassed with N$_2$ for 5 min and then heated at reflux under N$_2$ atmosphere for 24 h. After being cooled, the solid residue was filtered and washed with CH$_2$Cl$_2$ (50 mL). The organic filtrate was washed with water (100 mL × 2) and brine solution (100 mL), dried over anhydrous Na$_2$SO$_4$, and evaporated to dryness. Purification by silica gel column chromatography using CH$_2$Cl$_2$/hexane (1:9) as eluent gave a light gray solid (1.90 g, 44%): mp > 250 °C; ^{1}H NMR (300 MHz, CDCl$_3$, ppm) δ 8.37 (4H, s), 7.80 (2H, d, *J* = 7.2 Hz), 7.50–7.68 (16H, m), 7.20 (2H, d, *J* = 7.2 Hz), 1.67 (36H, s); ^{13}C NMR (75 MHz, CDCl$_3$, ppm) δ 147.2, 145.9, 145.6, 142.6, 139.4, 133.3, 130.9, 128.7, 127.8, 126.8, 125.3, 124.5, 123.6, 123.3, 122.7, 116.3, 110.8, 109.2, 34.8, 32.0; IR (KBr, cm^{-1}) ν 3042, 2955, 1507, 1483, 1312, 1295, 1262, 810; HRMS (ESI-TOF) m/z [M + H]$^+$ calcd for C$_{58}$H$_{61}$IN$_3$ 926.383, found 926.3902.

***N,N*-Bis(4-(3,6-di-*tert*-butylcarbazol-9-yl)phenyl)-4-(thiophen-2-yl)aniline (2).** A mixture of 1 (2.00 g, 1.9 mmol), 2-thiopheneboronic acid (0.27 g, 1.9 mmol), Pd(PPh$_3$)$_4$ (0.05 g, 0.04 mmol), and 2 M Na$_2$CO$_3$ aqueous solution (16 mL) in THF (40 mL) was degassed with N$_2$ for 5 min and then heated at reflux under N$_2$ atmosphere for 24 h. After being cooled, CH$_2$Cl$_2$ (100 mL) was added, and the organic phase was separated, washed with water (100 mL × 2) and brine solution (100 mL), dried over anhydrous Na$_2$SO$_4$, filtered, and evaporated to dryness. Purification by silica gel column chromatography using CH$_2$Cl$_2$/hexane (1:9) as eluent gave a light yellow solid (1.31 g, 72%): mp > 250 °C; ^{1}H NMR (300 MHz, CDCl$_3$, ppm) δ 8.11 (4H, d, *J* = 5.4 Hz), 7.59 (2H, s), 7.24–7.48 (20H, m), 7.05 (1H, s), 1.40 (36H, s); ^{13}C NMR (75 MHz, CDCl$_3$, ppm) δ 146.6, 145.9, 143.6, 142.7, 139.1, 132.7, 129.5, 128.5, 127.7, 121.1, 125.2, 124.9, 123.8, 123.1, 116.5, 109.5, 34.8, 32.2; IR (KBr, cm^{-1}) ν 3041, 2958, 1507, 1473, 1316, 1294, 1262, 809; HRMS (ESI-TOF) m/z [M + H]$^+$ calcd for C$_{62}$H$_{64}$N$_3$S 882.4743, found 882.4819.

4-(5-Bromothiophen-2-yl)-*N,N*-bis(4-(3,6-di-*tert*-butylcarbazol-9-yl)phenyl)aniline (3). N-Bromosuccinimide (0.35 g, 2.0 mmol) was added in small portions to a solution of 2 (1.71 g, 1.9 mmol) in THF (30 mL). The mixture was stirred at room temperature under N$_2$ for 1 h. Water (30 mL) and CH$_2$Cl$_2$ (100 mL) were added. The organic phase was separated, washed with water (100 mL × 2) and brine solution (100 mL), dried over anhydrous Na$_2$SO$_4$, filtered, and the solvents were removed to dryness. Purification by silica gel column chromatography eluting with CH$_2$Cl$_2$/hexane (1:9) gave brominated product as a light yellow solid (1.5 g, 91%): mp > 250 °C; ^{1}H NMR (300 MHz, CDCl$_3$, ppm) δ 8.15 (4H, d, *J* = 1.2 Hz), 7.26–7.52 (21H, m), 7.03 (1H, s), 1.48 (36H, s); ^{13}C NMR (75 MHz, CDCl$_3$, ppm) δ 147.3, 145.7, 142.9, 139.3, 138.5, 133.4, 127.7, 126.2, 125.2, 123.6, 123.3, 116.3, 109.2, 86.3, 34.7, 32.0; IR (KBr, cm^{-1}) ν 3041, 2959, 1507, 1316, 1294, 1263, 809; HRMS (ESI-TOF) m/z [M + H]$^+$ calcd for C$_{62}$H$_{63}$BrN$_3$S 960.3848, found 960.3908.

4-(2,2′-Bithiophen-5-yl)-*N,N*-bis(4-(3,6-di-*tert*-butylcarbazol-9-yl)phenyl)aniline (4). Compound 4 was synthesized as for 2 and obtained as a light yellow-green solid (63%): mp > 250 °C; ^{1}H NMR (300 MHz, CDCl$_3$, ppm) δ 8.16 (4H, s), 7.04–7.62 (25H, m), 1.48 (36H, s); ^{13}C NMR (75 MHz, CDCl$_3$, ppm) δ 146.7, 145.9, 142.8, 139.4, 133.2, 129.2, 127.8, 127.7, 126.7, 125.1, 124.6, 124.6, 124.6, 124.2, 123.9, 123.3, 123.2, 116.2, 109.2, 34.8, 32.0; IR (KBr, cm^{-1}) ν 3041, 2953, 1507, 1316, 1293, 1262, 808; HRMS (ESI-TOF) m/z [M + H]$^+$ calcd for C$_{66}$H$_{66}$N$_3$S$_2$ 964.4620, found 964.4637.

4-(5′-Bromo-2,2′-bithiophen-5-yl)-*N,N*-bis(4-(3,6-di-*tert*-butylcarbazol-9-yl)phenyl)aniline (5). Compound 5 was synthesized as for 3 and obtained as a yellow-green solid (87%): mp > 250 °C; ^{1}H NMR (300 MHz, CDCl$_3$, ppm) δ 8.16 (4H, s), 7.26–7.60 (21H, m), 7.18 (1H, d, *J* = 3.6 Hz), 7.09 (1H, d, *J* = 3.9 Hz), 6.98 (1H, d, *J* = 3.6 Hz), 6.94 (1H, d, *J* = 3.9 Hz), 1.49 (36H, s); ^{13}C NMR (75 MHz, CDCl$_3$, ppm) δ 147.0, 145.8, 143.3, 142.8, 139.3, 139.0, 135.0, 133.2, 130.6, 127.7, 126.8, 125.2, 124.9, 124.4, 123.5, 123.3, 123.1,

116.2, 109.2, 34.7, 32.0; IR (KBr, cm^{-1}) ν 3041, 2959, 1507, 1318, 1294, 1263, 808; HRMS (ESI-TOF) m/z [M + H]$^+$ calcd for C$_{66}$H$_6$5BrN$_3$S$_2$ 1042.3725, found 1042.3773.

4′-Bromo-*N*,*N*-bis(4-(3,6-di-*tert*-butylcarbazol-9-yl)phenyl)-1,1′-biphenyl-4-amine (6). Compound **6** was synthesized as for **2** and obtained as a colorless solid (76%): mp > 250 °C; ^{1}H NMR (300 MHz, CDCl$_3$, ppm) δ 8.16 (4H, s), 7.43−7.59 (21H, m), 1.48 (36H, s); ^{13}C NMR (75 MHz, CDCl$_3$, ppm) δ 142.85, 139.30, 131.90, 128.36, 127.70, 125.24, 123.34, 116.22, 109.31, 34.72, 32.06; IR (KBr, cm^{-1}) ν 2955, 1505, 1474, 1261, 808; HRMS (ESI-TOF) m/z [M + H]$^+$ calcd for C$_{64}$H$_{65}$BrN$_3$ 954.4362, found 954.4329.

4,4′-(*N*,*N*-Bis(4-(3,6-di-*tert*-butylcarbazol-9-yl)phenyl)-amino)-1,1′-biphenyl (BCPA). A mixture of **1** (0.71 g, 0.76 mmol), hexabutylditin (0.21 g, 0.37 mmol), and Pd(PPh$_3$)$_4$ (0.018 g, 0.015 mmol) in toluene (25 mL) was degassed with N$_2$ for 5 min and then heated at 80 °C under N$_2$ atmosphere for 24 h. After the reaction mixture was cooled to room temperature, water (10 mL) was added. The mixture was extracted with CH$_2$Cl$_2$ (50 mL × 2). The combined organic phase was washed with water (50 mL × 2) and brine solution (50 mL) and dried over anhydrous Na$_2$SO$_4$. It was then filtered and evaporated to dryness. Purification by silica gel column chromatography using CH$_2$Cl$_2$/hexane (1:6) as eluent followed by recrystallization with CH$_2$Cl$_2$/MeOH afforded a colorless solid (0.29 g, 51%): mp > 250 °C; ^{1}H NMR (300 MHz, CDCl$_3$, ppm) δ 8.16 (8H, s), 7.64 (4H, d, J = 8.1 Hz), 7.42−7.52 (36H, m), 1.54 (72H, s); ^{13}C NMR (75 MHz, CDCl$_3$, ppm) δ 145.2, 141.0, 140.6, 139.8, 139.3, 134.9, 134.9, 130.5, 129.9, 125.9, 125.5, 125.4, 124.3, 123.2, 123.1, 122.8, 117.6, 109.6, 34.4, 32.0; IR (KBr, cm^{-1}) ν 2958, 1505, 1474, 1261, 793; MALDI-TOF m/z [M + H]$^+$ calcd for C$_{116}$H$_{121}$N$_6$ 1597.965, found 1597.961.

2,5-Bis{*N*,*N*-bis-4-(3,6-di-*tert*-butylcarbazol-9-yl)phenyl4-aminophenyl}-9,9-dipropylfluorene (BCPA-F). Compound BCPA-F was synthesized as for **2** and obtained as a yellow solid (61%): mp > 250 °C; ^{1}H NMR (300 MHz, CDCl$_3$, ppm) δ 7.48−7.84 (46H, m), 2.13 (4H, m), 1.54 (74H, s), 0.78 (6H, m); ^{13}C NMR (75 MHz, CDCl$_3$, ppm) δ 146.7, 142.8, 139.4, 139.3, 136.8, 133.0, 128.3, 127.7, 125.7, 125.0, 123.3, 121.1, 120.1, 116.3, 109.3, 34.8, 32.0, 28.8, 24.4, 17.6; IR (KBr, cm^{-1}) ν 2952, 1507, 1493, 1262, 807; MALDI-TOF m/z [M]$^+$ calcd for C$_{135}$H$_{140}$N$_6$ 1845.114, found 1845.118.

2,5-Bis{*N*,*N*-bis4-(3,6-di-*tert*-butylcarbazol-9-yl)phenyl4-aminophenyl}thiophene (BCPA-T1). Compound BCPA-T1 was synthesized as for **2** and obtained as a yellow solid (65%): mp > 250 °C; ^{1}H NMR (300 MHz, CDCl$_3$, ppm) δ 8.16 (8H, s), 7.17−7.65 (42H, m), 1.48 (72H, s); ^{13}C NMR (75 MHz, CDCl$_3$, ppm) δ 146.6, 146.2, 142.8, 139.4, 139.4, 139.3, 136.8, 133.0, 128.3, 127.7, 125.7, 125.0, 123.3, 121.1, 120.1, 116.3, 109.3, 34.8, 32.1; IR (KBr, cm^{-1}) ν 2952, 1507, 1491, 1260, 786; MALDI-TOF m/z [M + H]$^+$ calcd for C$_{120}$H$_{123}$N$_6$S 1679.953, found 1679.950.

5,5′-Bis{*N*,*N*-bis4-(3,6-di-*tert*-butylcarbazol-9-yl)phenyl4-aminophenyl}-2,2′-bithiophene (BCPA-T2). Compound BCPA-T2 was synthesized as for BCPA and obtained as a light green solid (69%): mp > 250 °C; ^{1}H NMR (300 MHz, CDCl$_3$, ppm) δ (8H, d, J = 0.9 Hz), 7.61 (4H, d, J = 8.7 Hz), 7.40−7.53 (36H, m), 7.30 (4H, d, J = 8.4 Hz), 7.22 (2H, d, J = 3.6 Hz), 7.19 (2H, d, J = 3.6 Hz), 1.49 (72H, s); ^{13}C NMR (75 MHz, CDCl$_3$, ppm) δ 146.8, 145.9, 142.8, 139.3, 136.3, 133.2, 129.1, 127.7, 126.7, 125.1, 124.4, 123.5, 116.2, 109.2, 34.5, 32.0; IR (KBr, cm^{-1}) ν 2952, 1507, 1493, 1262, 807; MALDI-TOF m/z [M + H]$^+$ calcd for C$_{124}$H$_{125}$N$_6$S$_2$ 1761.941, found 1761.944.

5,5′′′-Bis{*N*,*N*-bis4-(3,6-di-*tert*-butylcarbazol-9-yl)phenyl4-aminophenyl}-2,2′:5′,2′′:5′′,2′′′-quaterthiophene (BCPA-T4). Compound BCPA-T4 was synthesized as for BCPA and obtained as an orange solid (73%): mp > 250 °C; ^{1}H NMR (300 MHz, CDCl$_3$, ppm) δ 8.16 (8H, d, J = 1.2 Hz), 7.60 (4H, d, J = 8.4 Hz), 7.40−7.53 (32H, m), 7.29 (4H, d, J = 8.4 Hz), 7.22 (2H, d, J = 3.7 Hz), 7.19 (2H, d, J = 3.7 Hz), 7.11 (4H, m), 1.49 (72H, s); ^{13}C NMR (75 MHz, CDCl$_3$, ppm) δ 146.9, 145.9, 143.0, 142.8, 139.3, 136.4, 133.2, 129.1, 127.7, 126.7, 125.2, 124.4, 123.5, 116.2, 109.2, 34.7, 32.0; IR (KBr, cm^{-1}) ν 2952, 1507, 1491, 1260, 808; MALDI-TOF m/z [M + H]$^+$ calcd for C$_{132}$H$_{129}$N$_6$S$_4$ 1925.916, found 1925.911.

4,7-Bis{*N*,*N*-bis4-(3,6-di-*tert*-butylcarbazol-9-yl)phenyl-aminophen-4-yl}-2,1,3-benzothiadiazole (BCPA-B). Compound BCPA-B was synthesized as for **2** and obtained as a red solid (79%): mp > 250 °C; ^{1}H NMR (300 MHz, CDCl$_3$, ppm) δ 8.16 (8H, s), 8.04 (4H, d, J = 8.4 Hz), 7.86, (2H, s), 7.43−7.55 (36H, m), 1.48 (72H, s); ^{13}C NMR (75 MHz, CDCl$_3$, ppm) δ 154.2, 147.6, 146.0, 142.8, 139.4, 132.2, 132.1, 130.3, 127.8, 127.7, 125.4, 123.9, 123.6, 123.3, 116.2, 109.2, 34.7, 32.0; IR (KBr, cm^{-1}) ν 2955, 1505, 1474, 1261, 808; MALDI-TOF m/z [M + H]$^+$ calcd for C$_{122}$H$_{123}$N$_8$S 1731.959, found 1731.957.

4,7-Bis{4,4′-(*N*,*N*-bis4-(3,6-di-*tert*-butylcarbazol-9-yl)phenyl-amino)-1,1′-biphenyl}-2,1,3-benzothiadiazole (BCPA-PB). Compound BCPA-PB was synthesized as for BCPA-B and obtained as a reddish-orange solid (68%): mp > 250 °C; ^{1}H NMR (300 MHz, CDCl$_3$, ppm) δ 8.16 (8H, d, J = 0.9 Hz), 8.10 (4H, d, J = 8.1 Hz), 7.90 (2H, s), 7.82 (4H, d, J = 8.1 Hz), 7.71 (4H, d, J = 8.4 Hz), 7.40−7.54 (36H, m), 1.49 (72H, s); ^{13}C NMR (75 MHz, CDCl$_3$, ppm) δ 154.2, 142.8, 139.3, 136.0, 133.2, 132.8, 129.7, 128.2, 127.7, 127.0, 125.1, 124.6, 123.5, 123.3, 123.3, 116.2, 109.2, 34.7, 32.0; IR (KBr, cm^{-1}) ν 2958, 1505, 1474, 1261, 814, 793; MALDI-TOF m/z [M + H]$^+$ calcd for C$_{134}$H$_{131}$N$_8$S 1884.022, found 1884.018.

4,7-Bis{5-(*N*,*N*-bis4-(3,6-di-*tert*-butylcarbazol-9-yl)phenyl-aminophenyl)-thien-2-yl}-2,1,3-benzothiadiazole (BCPA-TB). Compound BCPA-TB was synthesized as for **2** and obtained as a dark red solid (58%): mp > 250 °C; ^{1}H NMR (300 MHz, CDCl$_3$, ppm) δ 8.17 (8H, s), 7.90 (2H, s), 7.71 (4H, d, J = 8.2 Hz), 7.40−7.55 (36H, m), 7.32 (4H, d, J = 8.2 Hz), 1.49 (72H, s); ^{13}C NMR (75 MHz, CDCl$_3$, ppm) δ 152.6, 147.1, 145.9, 145.2, 142.8, 139.4, 133.2, 129.1, 128.7, 127.8, 127.0, 125.4, 125.2, 124.4, 123.9, 123.3, 123.3, 116.2, 109.2, 34.7, 32.0; IR (KBr, cm^{-1}) ν 2958, 1505, 1474, 1261, 814, 793; MALDI-TOF m/z [M + H]$^+$ calcd for C$_{130}$H$_{127}$N$_8$S$_3$ 1895.935, found 1895.933.

Optical, Thermal, Electrochemical, and Physical Characterizations. UV−vis absorption and photoluminescence spectra were recorded as a dilute solution in spectroscopic grade CH$_2$Cl$_2$ and thin film obtained by spin-casting. The fluorescence quantum yields (Φ_F) were determined by comparison with a fluorescence standard of quinine sulfate in 0.01 M % H$_2$SO$_4$ (Φ_F = 0.54) and coumarin 6 in ethanol (Φ_F = 0.78).[35] Differential scanning calorimetry (DSC) analysis and thermogravimetric analysis (TGA) were analyzed with a heating rate of 10 °C min^{-1} under a N$_2$ atmosphere. Cyclic voltammetry (CV) and differential pulse voltammetry (DPV) measurements were carried out with a three-electrode system (platinum counter electrode, glassy carbon working electrode, and Ag/Ag$^+$ reference electrode) at a scan rate of 50 mV s^{-1} in CH$_2$Cl$_2$ under an Ar atmosphere. The concentration of analytical materials and tetrabutyl ammonium hexafluorophosphate (n-Bu$_4$NPF$_6$) were 10^{-3} and 0.1 M, respectively. The atomic force microscopy (AFM) analysis was performed using standard noncontact mode with a resonance of 316.17 kHz.

Quantum Computer Calculation. The ground state geometries of BCPA-Ars were fully optimized using density functional theory (DFT) at the B3LYP/6-31G(d,p) level, as implemented in Gaussian 09.[14] The TDDFT/B3LYP calculation of the lowest excitation energies was performed at the optimized geometries of the ground states.

Device Fabrication and Testing. OLED devices using BCPA-Ars as a nondoped missive layer (EML) with the device configurations of ITO/PEDOT:PSS/BCPA-Ar(spin-coating)/LiF(0.5 nm):Al(150 nm) and ITO/PEDOT:PSS/BCPA-Ar(spin-coating)/BCP(40 nm)/LiF-(0.5 nm):Al(150 nm) were fabricated and characterized as follows. The patterned indium tin oxide (ITO) glass substrate with a sheet resistance a 14 ohm sq^{-1} was thoroughly cleaned by successive ultrasonic treatments in detergent, deionized water, isopropanol, and acetone and then dried at 60 °C in a vacuum oven. A 50 nm thick PEDOT/PSS hole-injection layer was spin-coated on top of ITO from a 0.75 wt % dispersion in water at a spin speed of 3000 rpm for 20 s and dried at 200 °C for 15 min under vacuum. Thin films of BCPA-Ars were deposited on top of PEDOT/PSS layer by spin-coating in a CHCl$_3$/toluene solution (5:1) of BCPA-Ars (1.5% w/v) at a spin

speed of 3000 rpm for 30 s to create a film thickness of 30−40 nm. The film thickness was measured using a Tencor π-Step 500 surface profiler. For the double-layer device, BCP was deposited onto the surface of the BCPA-Ars film as an electron-transporting layer (ETL) with a thickness of 40 nm by evaporating from resistively heated alumina crucibles at an evaporation rate of 0.5−1.0 nm s^{-1} in vacuum evaporator deposition (ES280, ANS Technology) under a base pressure of ≈10^{-5} mbar. The film thickness was monitored and recorded by a quartz oscillator thickness meter (TM-350, MAXTEK). The chamber was vented with dry air to load the cathode materials and pumped back; a 0.5 nm thick LiF and a 150 nm thick aluminum (Al) layer were subsequently deposited through a shadow mask on the top of EML or BCP films without breaking vacuum to form active diode areas of 4 mm^2. The measurement of device efficiency was performed according to M.E. Thompson's protocol, and the device external quantum efficiencies were calculated using procedure reported previously.[36] Current density−voltage−luminescence ($J−V−L$) characterisics were measured simultaneously using a Keithley 2400 source meter and a Newport 1835C power meter equipped with a Newport 818-UV/CM calibrated silicon photodiode. The EL spectra were acquired by an Ocean Optics USB4000 multichannel spectrometer. All the measurements were performed under ambient atmosphere at room temperature immediately after breaking the chamber.

ASSOCIATED CONTENT

Supporting Information

AFM images, DFT calculations data, CV curves, DSC/TGA thermograms, OLED devices data, and NMR spectra. This material is available free of charge via the Internet at http://pubs.acs.org.

AUTHOR INFORMATION

Corresponding Author
*E-mail: pvinich@sut.ac.th.

Notes
The authors declare no competing financial interest.

ACKNOWLEDGMENTS

REFERENCES

(1) Tang, C. W.; VanSlyke, S. A. *Appl. Phys. Lett.* **1987**, *51*, 913.

(2) (a) Wu, C.-C.; Chen, C.-W.; Lin, C.-L.; Yang, C.-J. *J. Disp. Technol.* **2005**, *1*, 248. (b) Geffroy, B.; le Roy, P.; Prat, C. *Polym. Int.* **2006**, *55*, 572. (c) So, F.; Kido, J.; Burrows, P. L. *MRS Bull.* **2008**, *33*, 663.

(3) (a) Duan, L.; Hou, L.; Lee, T.-W.; Qiao, J.; Zhang, D.; Dong, G.; Wang, L.; Qiu, Y. *J. Mater. Chem.* **2010**, *20*, 6392. (b) Zhu, X.-H.; Peng, J.; Cao, Y.; Roncali, J. *Chem. Soc. Rev.* **2011**, *40*, 3509.

(4) (a) Chang, C.-J.; Yang, C.-H.; Chen, K.; Chi, Y.; Shu, C.-F.; Ho, M.-L.; Yeh, Y.-S.; Chou, P.-T. *Dalton Trans.* **2007**, 1881. (b) Hwang, F. M.; Chen, H. Y.; Chen, P. S.; Liu, C. S.; Chi, Y. C.; Shu, C. F.; Wu, F. L.; Chou, P. T.; Peng, S. M.; Lee, G. H. *Inorg. Chem.* **2005**, *44*, 1344. (c) Kim, E.; Park, S. B. *Chem.—Asian J.* **2009**, *4*, 1646.

(5) (a) Andersson, M. R.; Thomas, O.; Mammo, W.; Svensson, M.; Theander, M.; Inganäs, O. *J. Mater. Chem.* **1999**, *9*, 1933. (b) Andersson, M. R.; Berggren, M.; Inganäs, O.; Gustafsson, G.; Gustaffson-Carlberg, J. C.; Selse, D.; Hjertberg, T.; Wennerström, O. *Macromolecules* **1995**, *28*, 7525.

(6) (a) Ahn, T.; Sik Jang, M.; Shim, H.-K.; Hwang, D.-H.; Zyung, T. *Macromolecules* **1999**, *32*, 3279. (b) Anderson, M. R.; Yu, G.; Heeger,

A. J. *Synth. Met.* **1997**, *85*, 1275. (c) Akcelrud, L. *Prog. Polym. Sci.* **2003**, *28*, 875.

(7) Wee, K.-R.; Ahn, H.-C.; Son, H.-J.; Han, W.-S.; Kim, J.-E.; Cho, D. W.; Kang, S. O. *J. Org. Chem.* **2009**, *74*, 8472.

(8) Ahn, T.; Sik Jang, M.; Shim, H.-K.; Hwang, D.-H.; Zyung, T. *Chem. Mater.* **2005**, *17*, 5032.

(9) (a) Pohl, R.; Montes, V. A.; Shinar, J.; Anzenbacher, P., Jr. *J. Org. Chem.* **2004**, *69*, 1723. (b) Pohl, R.; Anzenbacher, P., Jr. *Org. Lett.* **2003**, *5*, 2769. (c) Montes, V. A.; Li, G.; Pohl, R.; Shinar, J.; Anzenbacher, P., Jr. *Adv. Mater.* **2004**, *16*, 2001.

(10) (a) Coppo, P.; Plummer, E. A.; Cola, L. D. *Chem. Commun.* **2004**, 1774. (b) Lamansky, S.; Djarovich, P.; Murphy, D.; Razzaq, F. A.; Kwong, R.; Tsyba, I.; Bortz, M.; Mui, B.; Bau, R.; Thompson, M. E. *Inorg. Chem.* **2001**, *40*, 1704.

(11) (a) Moonsin, P.; Prachumrak, N.; Rattanawan, R.; Keawin, T.; Jungsuttiwong, S.; Sudyoadsuk, T.; Promarak, V. *Chem. Commun.* **2012**, *48*, 3382. (b) Promarak, V.; Ichikawa, M.; Sudyoadsuk, T.; Saengsuwan, S.; Jungsuttiwong, S.; Keawin, T. *Synth. Met.* **2007**, *157*, 17. (c) Li, J.; Ma, C.; Tang, J.; Lee, C.-S.; Lee, S. *Chem. Mater.* **2005**, *17*, 615. (d) He, Q.; Lin, H.; Weng, Y.; Zhang, B.; Wang, Z.; Lei, G.; Wang, L.; Qiu, Y.; Bai, F. *Adv. Funct. Mater.* **2006**, *16*, 1343.

(12) Meunmart, D.; Prachumrak, N.; Keawin, T.; Jungsuttiwong, S.; Sudyoadsuk, T.; Promarak, V. *Tetrahedron Lett.* **2012**, *53*, 3615.

(13) Khunchalee, J.; Tarsang, R.; Prachumrak, N.; Jungsuttiwong, S.; Keawin, T.; Sudyoadsuk, T.; Promarak, V. *Tetrahedron* **2012**, *68*, 8416.

(14) Frisch, M. J.; Trucks, G. W.; Schlegel, H. B.; Scuseria, G. E.; Robb, M. A.; Cheeseman, J. R.; Scalmani, G.; Barone, V.; Mennucci, B.; Petersson, G. A.; Nakatsuji, H.; Caricato, M.; Li, X.; Hratchian, H. P.; Izmaylov, A. F.; Bloino, J.; Zheng, G.; Sonnenberg, J. L.; Hada, M.; Ehara, M.; Toyota, K.; Fukuda, R.; Hasegawa, J.; Ishida, M.; Nakajima, T.; Honda, Y.; Kitao, O.; Nakai, H.; Vreven, T.; Montgomery, J. A., Jr.; Peralta, J. E.; Ogliaro, F.; Bearpark, M.; Heyd, J. J.; Brothers, E.; Kudin, K. N.; Staroverov, V. N.; Kobayashi, R.; Normand, J.; Raghavachari, K.; Rendell, A.; Burant, J. C.; Iyengar, S. S.; Tomasi, J.; Cossi, M.; Rega, N.; Millam, J. M.; Klene, M.; Knox, J. E.; Cross, J. B.; Bakken, V.; Adamo, C.; Jaramillo, J.; Gomperts, R.; Stratmann, R. E.; Yazyev, O.; Austin, A. J.; Cammi, R.; Pomelli, C.; Ochterski, J. W.; Martin, R. L.; Morokuma, K.; Zakrzewski, V. G.; Voth, G. A.; Salvador, P.; Dannenberg, J. J.; Dapprich, S.; Daniels, A. D.; Farkas, Ö.; Foresman, J. B.; Ortiz, J. V.; Cioslowski, J.; Fox, D. J. *Gaussian 09*, revision A.1; Gaussian, Inc.: Wallingford, CT, 2009.

(15) Ning, Z. J.; Zhou, Y. C.; Zhang, Q.; Ma, D. G.; Zhang, J. J.; Tian, H. *J. Photochem. Photobiol. A: Chem.* **2007**, *192*, 8.

(16) Collado, D.; Casado, J.; Rodríguez González, S.; López Navarrete, J. T.; Suau, R.; Perez-Inestrosa, E.; Pappenfus, T. M.; Raposo, M. M. *Chem.—Eur. J.* **2011**, *17*, 498.

(17) Promarak, V.; Punkvuang, A.; Sudyoadsuk, T.; Jungsuttiwong, S.; Saengsuwan, S.; Keawin, T.; Sirithip, K. *Tetrahedron* **2007**, *83*, 8881.

(18) Khunchalee, J.; Tarsang, R.; Jungsuttiwong, S.; Keawin, T.; Sudyoadsuk, T.; Promarak, V. *Tetrahedron Lett.* **2012**, *53*, 5939.

(19) (a) Linton, K. E.; Fisher, A. L.; Pearson, C.; Fox, M. A.; Pålsson, L.-O.; Bryce, M. R.; Petty, M. C. *J. Mater. Chem.* **2012**, *22*, 11816. (b) Promarak, V.; Punkvuang, A.; Jungsuttiwong, S.; Saengsuwan, S.; Sudyoadsuk, T.; Keawin, T. *Tetrahedron Lett.* **2007**, *48*, 3661. (c) Albers, W. M.; Canters, G. W.; Reedijk, J. *Tetrahedron* **1995**, *51*, 3895.

(20) Noda, T.; Imae, I.; Noma, N.; Shirota, Y. *Adv. Mater.* **1997**, *9*, 239.

(21) Xia, P. F.; Lu, J.; Kwok, C. H.; Fukutani, H.; Wong, M. S.; Tao, Y. *J. Polym. Sci., Part A: Polym. Chem.* **2009**, *47*, 137.

(22) Fink, R.; Heischkel, Y.; Thelakkat, M.; Schmidt, H. *Chem. Mater.* **1998**, *10*, 3620.

(23) Kuo, T.-W.; Chung, H.-P.; Chen, T.-M. *Chem. Lett.* **2010**, *39*, 200.

(24) Takada, K.; Ichimura, M.; Ishibashi, T.; Tamura, S. JP2001131128, 2001.

(25) Yeh, H.-C.; Yeh, S.-J.; Chen, C.-T. *Chem. Commun.* **2003**, 2632.

(26) Thomas, K. R. J.; Lin, J. T.; Tao, Y.; Chuen, C. *Adv. Mater.* **2002**, *114*, 822.

(27) Tang, C.; Liu, F.; Xia, Y.-J.; Lin, J.; Xie, L.-H.; Zhong, G.-Y.; Fan, Q.-L.; Huang, W. *Org. Electron.* **2006**, *7*, 155.

(28) Kim, D. Y.; Cho, H. N.; Kim, C. Y. *Prog. Polym. Sci.* **2000**, *25*, 1089.

(29) (a) Li, Q.; Li, J.; Yang, R.; Deng, L.; Gao, Z.; Liu, D. *Dyes Pigm.* **2012**, *92*, 674. (b) Li, J.; Duan, Y.; Li, Q. *Dyes Pigm.* **2013**, *96*, 391. (c) Zhang, M.; Xue, S.; Dong, W.; Wang, Q.; Fei, T.; Gu, C.; Ma, Y. *Chem. Commun.* **2010**, *46*, 3923.

(30) (a) Wang, Z.; Lu, P.; Xue, S.; Gu, C.; Lv, Y.; Zhu, Q.; Wang, H.; Ma, Y. *Dyes Pigm.* **2011**, *91*, 356. (b) Yang, Y.; Zhou, Y.; He, Q.; He, C.; Yang, C.; Bai, F.; Li, Y. *J. Phys. Chem. B* **2009**, *113*, 7745. (c) Li, J.; Li, Q.; Liu, D. *ACS Appl. Mater. Interfaces* **2011**, *3*, 2099. (d) Pan, J. F.; Zhu, W. H.; Li, S. F.; Zeng, W. J.; Cao, Y.; Tian, H. *Polymer* **2005**, *46*, 7658. (e) Kim, G. W.; Cho, M. J.; Yu, Y. J.; Kim, Z. H.; Jin, J.; Kim, D. Y.; Choi, D. H. *Chem. Mater.* **2007**, *19*, 42. (f) Burn, P. L.; Lo, S.-C.; Samuel, I. D. W. *Adv. Mater.* **2007**, *19*, 1675. (g) Wang, J. L.; Zhou, Y.; Li, Y. F.; Pei, J. *J. Org. Chem.* **2009**, *74*, 7449.

(31) (a) Justin Thomas, K. R.; Lin, J. T.; Velusamy, M.; Tao, Y.-T.; Chuen, C.-H. *Adv. Funct. Mater.* **2004**, *14*, 83. (b) Yeh, H.; Chan, L.; Wua, W.; Chen, C. *J. Mater. Chem.* **2004**, *14*, 1293. (c) Chen, C. *Chem. Mater.* **2004**, *16*, 4389. (d) Yeh, H.-C.; Yeh, S.-J.; Chen, C.-T. *Chem. Commun.* **2003**, 2632.

(32) Im, W. B.; Hwang, H. K.; Lee, J. G.; Han, K.; Kim, Y. *Appl. Phys. Lett.* **2001**, *79*, 1387.

(33) Wu, W.-C.; Liu, C.-L.; Chen, W.-C. *Polymer* **2006**, *47*, 527.

(34) (a) Kim, Y. K.; Hwang, S.-H. *Synth. Met.* **2006**, *156*, 1028. (b) Thaengthong, A.; Saengsuwan, S.; Jungsuttiwong, S.; Keawin, T.; Sudyoadsuk, T.; Promarak, V. *Tetrahedron Lett.* **2011**, *52*, 4749.

(35) (a) Kartens, T.; Kobs, K. *J. Phys. Chem.* **1980**, *84*, 1871. (b) Ammar, H.; Fery-Forgues, S.; Gharbi, R. E. *Dyes Pigm.* **2003**, *57*, 259.

(36) Forrest, S. R.; Bradley, D. D. C.; Thompson, M. E. *Adv. Mater.* **2003**, *15*, 1043.